EXPERIMENTAL AND NUMERICAL STUDY OF THE INFLUENCE OF TEMPERING TEMPERATURE ON THE TENSILE BEHAVIOR OF LOW ALLOY STEEL AISI 4140

Abdelmalek ELHADI[1], Salah AMROUNE[1*], Amin HOUARI[2,3], Mohamed SLAMANI[1], Madani KOUIDER[3]

Understanding the mechanical properties of steel is crucial to ensuring the proper functioning of industrial mechanical systems. This study focuses on the tensile behavior and specific mechanical properties of low-alloy steel AISI 4041. It combines practical experiments and numerical simulations using Abaqus software. The experiments involve fabricating 18 standard-sized tensile specimens, followed by a heat treatment including oil quenching and various tempering temperatures (ranging from 350°C to 650°C) to create a range of hardness levels. Tensile tests provided experimental data, subsequently validated by numerical analyses using the eXtended Finite Element Method (XFEM). The results indicate a maximum hardness of 522 HV, maximum tensile load and a maximum tensile strength of 1680 MPa with tempering at 350°C. This approach significantly improved the results, with errors generally below 0.06% for maximum strain and stress. This study provides valuable insights for designing and optimizing low-alloy steel structures suitable for high-temperature environments.

Keywords: Low alloy steel, quenching, tempering, hardness, tensile test, tensile strength

1. Introduction

Steels in general are commonly used in industrial applications. Low-alloy steels are the most widely used materials for the manufacture of mechanism components used in industry such as automobile industry and machine elements because of their high mechanical properties and operating life [1-6]. They are generally used in the quenched and tempered condition. The tempering heat treatment is carried out after quenching, with the aim of changing the martensitic

[1] Laboratory of Materials and Mechanics of Structures (LMMS), Faculty of technology, University of Msila, PO. Box. 166 Ichebilia 28000 Msila, Algeria, e-mail: salah.amroune@univ-msila.dz
[2] Laboratory of Motor Dynamics and Vibroacoustics (LDMV), Department of Mechanical Engineering, Mhamed Bougara University of Boumerdes, Boumerdes, Algeria, e-mail: a.houari@univ-boumerdes.dz
[3] Laboratoire de Matériaux et Mécanique des Structures (LMMS), Université SBA. Sidi Bel Abesse, Algérie, e-mail : kouider.madani@univ-sba.dz

or martensito-bainitic structure obtained after quenching, so as to have sufficient ductility, resilience and satisfactory toughness [7].

Many authors [8-10] have studied the effect of quenching and tempering heat treatment on the mechanical properties of low alloy steels. It helps to control the mechanical properties of steel by reducing its hardness and tensile strength, but increasing its ductility [11-13]. The tensile test makes it possible to determine many standardized quantities of the mechanical properties, such as yield strength, elongation and maximum tensile strength. These quantities are necessary in the calculations of the structures. Another experimental study conducted by Sharma et al [14], investigates the transition from ductile to brittle behavior in a bainitic steel. Researchers conducted experiments and molecular dynamics simulations. Experimental findings showed that fracture facets changed from {100} to off-{100} with increasing temperature, associated with a shift in fracture mode. Simulations revealed that the intrinsic cleavage plane remained {100}, but atomistic mechanisms of crack kinking and dislocation pile-up at higher temperatures created off- {100} facets. This study combines experimentation and modelling to explain the transition from ductile to brittle behavior. A different experiment was conducted by Buchmayr and Kirkaldy [15], in which the authors have developed a comprehensive finite element program applicable to all axisymmetric shapes for predicting the behavior of materials subjected to various heat treatments. This program is based on a thermodynamic and kinetic, algorithm for predicting the hardenability of low alloy steels, coupled with the calculation of stress and strain evolution. During the temperature field and stress calculations, microstructural contributions, such as latent heat formation, influence on thermophysical properties, microstructural dependence of the σ/ε curve, transformation strain, and transformation plasticity are considered. This provides deeper insights and more accurate predictions of material response. As a result, microstructural optimizations with respect to hardenability, hardness, residual stresses, and distortion become feasible. A study that integrates both numerical and experimental approaches, was led by Benzing et al [16], The authors examine the room temperature tensile properties of a medium-Mn TWIP-TRIP (Twinning Induced Plasticity and Transformation Induced Plasticity) steel across various strain rates. The multi-phase material shows positive strain-rate sensitivity. They use empirical data and a finite-element model to analyse microstructural influences on mechanical properties, offering insights for alloy design.

As a result of the aforementioned work, the originality of our study consists of multidisciplinary approach, combining experimentation and numerical simulation to delve deeply into the mechanical properties of low-alloy steel AISI 4041. This innovative approach yields acceptable accuracy precise results, with errors generally below 15% in terms of maximum strain and stress. Furthermore, this research goes beyond the traditional analysis of mechanical properties by

investigating the impact of thermal treatments on the material, particularly quenching and tempering at various temperatures, thereby enriching the understanding of the behavior mechanisms of the studied steel. The fabrication of 12 standard-sized samples and the utilization of advanced simulation software, Abaqus, bring both experimental and numerical rigor to the study. Experimental data is subsequently validated through numerical analyses based on the eXtended Finite Element Method (XFEM), representing a sophisticated approach for result validation. This research provides an innovative and comprehensive perspective on the mechanical properties of low-alloy steel AISI 4041, with valuable implications for the design and optimization of steel structures intended for high-temperature environments. It should be noted that the experimental results obtained are processed and analyzed by the Abaqus software in order to make a comparison between the experimental and numerical results.

2. Material and experimental devices used

The material used for the tensile specimen is a low alloy steel AISI 4140, intended mainly for the manufacture of medium to large section parts: shafts, axles, racks, crankshafts, connecting rods, gears. Its average hardness is 310 HV in the delivered state (untreated), it presents a good compromise between hardness and resilience in the quenched and tempered state.

The chemical composition of the material studied by spectroscopy is indicated in Table 1.

Table 1

Chemical composition of the material (wt%)

C	Cr	Mn	Mo	Si	Cu	Co	P
0.40	1.06	0.81	0.18	0.20	0.16	0.13	0.035

Thermal treatment of the material consists of:

a): Heat the specimens to temperature of 830°C.

b): Maintain at this temperature for about 30 minutes to allow complete austenization.

c): Quick cool the specimens, by dipping in oil.

d): Heating at different tempering temperatures (350°C, 450°C, 550°C and 650°C) after quenching and a holding time of 30min and air cooling to ambient temperature.

Fig 1 shows the untreated and heat treated tensile specimens.

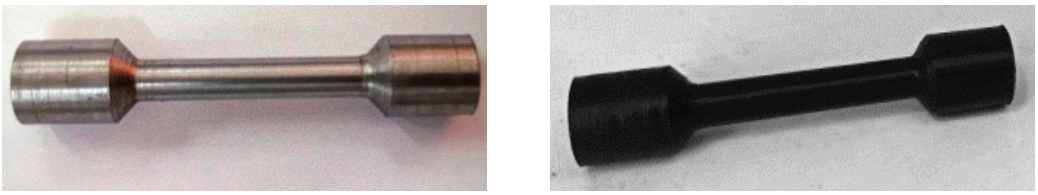

(a) (b)

Fig. 1. Tensile specimens: a) Before heat treatment; b) After heat treatment

The tensile machine used is a hydraulically driven column vertical testing device (Fig 2). The maximum pulling force can reach 50 KN in both directions. It is equipped with a PC for entering and acquiring data and information relating to the specimen and the machine. 15 specimens were machined for the tensile tests to be carried out. Three identical specimens (tempered at the same temperature) were tested to average the results. The strain rate at which the tests were carried out is 2 mm/min.

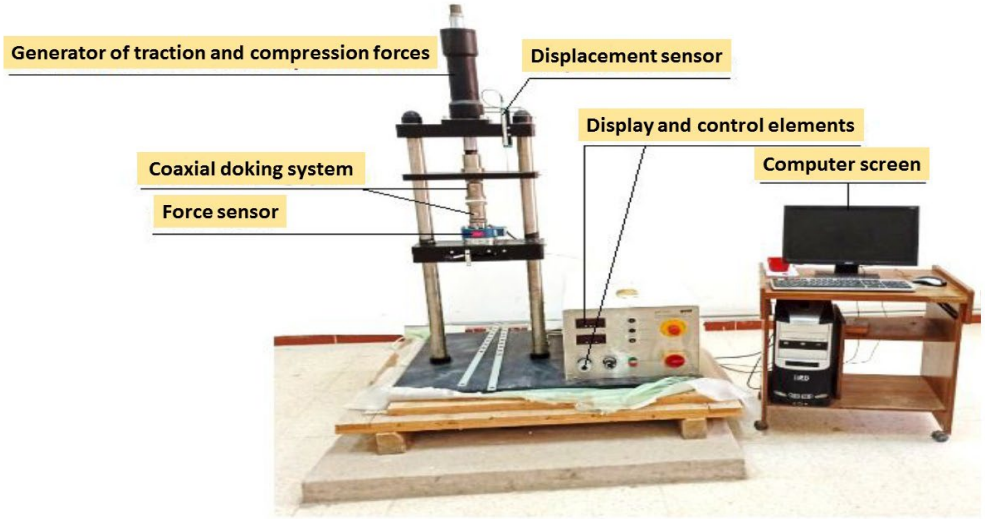

Fig. 2. Traction machine used (WP 310)

The geometry and the dimensions (in mm) of the tensile specimens is according to the ISO 6892-1 standard shown in the Fig 3.

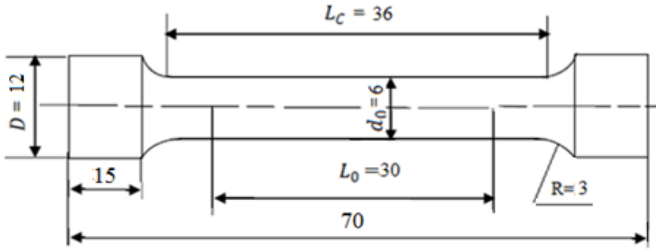

Fig. 3. Tensile specimen used.

3. Results and discussion

3.1. *Variation of the hardness as a function of tempering temperature*

The variation of hardness as a function of tempering temperature is shown in Fig 4. The hardness of the material gradually decreases from 522 HV to 304 HV with increasing tempering temperatures from 350°C to 650°C

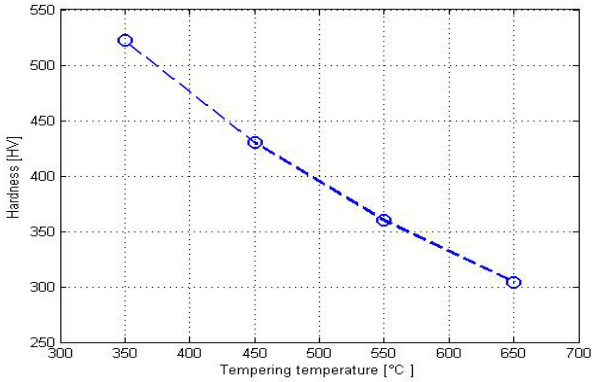

Fig. 4. Variation of the hardness as a function of tempering temperature

3.2. *Variation of tensile load and tensile strength as a function of tempering temperature*

Fig. 5 shows the influence of tempering temperature on load and tensile strength. The Figs 5a and 5b show the decrease in tensile load and tensile strength with increasing of the tempering temperature. The material tempered at 350°C recorded a maximum tensile load of 46.66 kN (Fig 5a), which corresponds to a maximum tensile strength of 1680 MPa (fig 5b). Tempering temperature at reduced 650°C gave minimum values of tensile load 25.72 kN and tensile strength of steel at a value of 926 MPa.

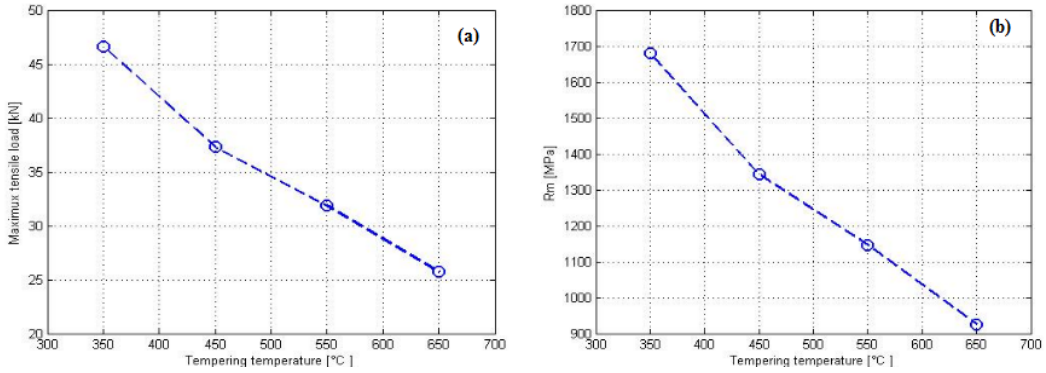

Fig. 5. Variation of: (a) tensile load (b) tensile strength as a function of tempering temperature

3. 3. *Variation of percent elongation A% as a function of tempering temperature*

Fig. 6 shows that the value of the percent elongation A% of the material is maximum at the tempering temperature of 650°C and minimum at the tempering temperature of 350°C. The influence of the tempering temperature is not really significant between 350°C and 450°C but it became strong after temperature 450°C up to temperature 650°C.

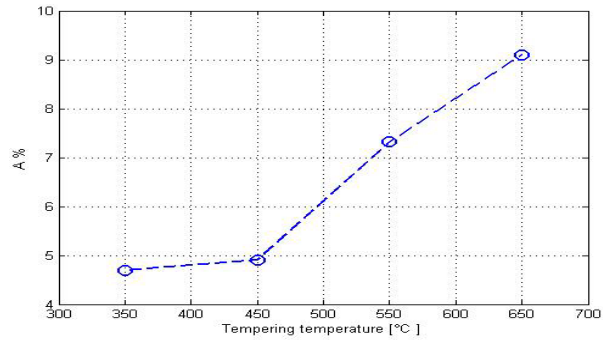

Fig. 6. Variation of elongation as a function of tempering temperature

The tempering temperature has a greater influence on the change in mechanical properties [17]. The different hardness values obtained as a function of the tempering temperature between 350°C and 650°C with a step of 100°C for a holding time of 30 min, correspond to the studies presented by the authors [18, 19]. The quenching heat treatment (heating to a temperature of 830°C then rapid cooling of the steel) promotes the formation of martensite which is characterized by its fine and tight crystalline plates or lamellae which make the steel hard but fragile. This fragility is due to residual stresses in the crystal structure of the steel. Tempering

treatment is necessary to eliminate internal stresses due to the disorganization of atoms in the material during rapid cooling which do not have sufficient time to reorganize into a stable crystal structure. This tempering treatment balances the hardness and toughness of the steel and makes it more suitable for certain industrial applications. Increasing the tempering temperature results in a significant decrease in hardness [14, 19], the decrease in tensile strength of the material and consequently, a reduction in the elastic limit.

At lower tempering temperatures, steel can become more brittle, meaning it is more likely to fail in a brittle manner rather than undergoing significant plastic deformation before failure. This generally results in a decrease in percent elongation.

the increase in percent elongation with increasing tempering temperature is explained by certain metallurgical precipitates or phases that can dissolve and low dislocation density with reduced work hardening rate [20-22].

Furthermore, increasing the tempering temperature above 450°C promotes the diffusion of atoms, the carbon dissolved in the crystalline matrix during hardening precipitates in the form of iron carbides which reduces the hardness [23, 19] and significant increase in elongation. The increase in the percentage of addition elements such as Mn (0.81%) and Cr (1.06%) justifies the notable increase in the hardness of the material in the untreated state [24, 25]. The fracture of the samples is ductile, characterized by the presence of macroscopic plastic deformation, and therefore by the slow propagation of cracks with high energy consumption. Fracture ductility may be desired by the designer.

3.4. *Thermoelastic constitutive equations*

For the numerical analysis of our study, we used a most general mathematical formulation for the mechanical and thermal effects on the stress analysis in steels. When the material passes over the elastic domain, we can say that this material is in inelastic phase therefore the thermoelastic relationship between the strain and stress components is defined by Hooke's law as follows:

$$\varepsilon^{el} - \varepsilon^{th} = \frac{(1+\nu)}{E}\sigma_{ij} - \frac{(1+\nu)}{E}\sigma_{ij}I \quad (1)$$

The total strain ε is the strain caused by thermal expansion. This form of strain decomposition depends on the measurement of the integrated strain rate and the weakness of elastic and thermal strains. These standard models of plasticity are provided in the program. From the equation above, we can deduce the deformations due to these two effects to give us the total deformation such that:

$$\varepsilon^{el} - \varepsilon^{th} = \varepsilon - \varepsilon^{pl} \; and \; \varepsilon^{th} = \alpha.\Delta T \quad (2)$$

ε is the total strain, ε^{el} is the mechanical elastic strain, ε^{pl} is the mechanical plastic strain and ε^{th} is the thermal strain. In the constitutive models in ABAQUS

$\varepsilon^{th} = \varepsilon^{th}(\theta)$ [26]. The equation for thermal strain is $\varepsilon^{th} = \alpha.\Delta T$, where α is the coefficient of thermal expansion and $\Delta T = T - T_i$ is the time duration of temperature exposure, where T and T_i respectively the temperature and the initial temperature. Then, we defined the plastic flow is integrated by the retrospective Euler method to give:

$$\Delta\varepsilon^{pl} = \Delta\bar{\varepsilon}^{pl} n \tag{3}$$

where $\bar{\varepsilon}^{pl}$ is a scalar measure of plastic strain that is used as a hardening parameter in the definitions of yield surface and flow potential in some plasticity models and n is the direction of flow, defined as follows:

$$n = \frac{3S}{2q} \; and \; q = \sqrt{\frac{2}{3}S.S} \tag{4}$$

The plasticity requires that the material satisfy an uniaxial-stress plastic-strain strain-rate relationship. If the material is rate independent, this is the yield condition:

$$q = \sigma^0\left(\bar{\varepsilon}^{pl}, \theta\right) \tag{5}$$

where $\sigma^0\left(\bar{\varepsilon}^{pl}, \theta\right)$ is the yield stress and is defined by the user as a function of equivalent plastic strain ($\bar{\varepsilon}^{pl}$) and temperature (θ). while $q = h.\sigma^0$ for a rate-dependent model, where:

$$h = h\left(\frac{\Delta\varepsilon^{pl}}{\Delta t}, \theta\right) \tag{6}$$

where h is a known function. If the material is rate dependent, the relationship is the uniaxial flow rate definition:

$$\dot{\bar{\varepsilon}}^{pl} = h(q, \bar{\varepsilon}^{pl}, \theta) \tag{7}$$

For example, the rate-dependent material model offers an overstress power law model of the form:

$$\dot{\bar{\varepsilon}}^{pl} = D\left(\frac{q}{\sigma^0} - 1\right)^n \tag{8}$$

where $D(\theta)$ and $n(\theta)$ are user-defined temperature-dependent material parameters. Using the average plastic strain rate over the increment in this expression defines:

$$h = 1 + \left(\frac{\Delta\varepsilon^{pl}}{D\Delta t}\right)^{1/n} \tag{9}$$

Integrating this relation by the backward Euler method gives (equation 10).

$$\Delta\bar{\varepsilon}^{pl} = \Delta t.\, h\left(q, \bar{\varepsilon}^{pl}, \theta\right) \tag{10}$$

This equation can be inverted (numerically, if necessary) to give q as a function of $\bar{\varepsilon}^{pl}$ at the end of the increment. Thus, both the rate-independent model and the integrated rate-dependent model give the general uniaxial form:

$$q = \bar{\sigma}\left(\bar{\varepsilon}^{pl}\right) \tag{11}$$

where $\bar{\sigma} = \sigma^0$ for the rate-independent model and $\bar{\sigma}$ is obtained by inversion of equation (10) for the rate-dependent model.

3.5. *Damage model*

Damage in isotropic materials is widely used with different plasticity models following their simple execution. To this end, continuous damage mechanics has become a promising tool for the description of the degradation of materials by internal state variables D, scalar or tensor depending on the objective to be achieved during modeling, this variable measures the stiffness degradation defined between 0 for an undamaged material and 1 for a totally damaged material, given by [27]:

$$\sigma_{ij} = (1 - D)C_{ijkl}\varepsilon_{kl} \tag{12}$$

Therefore, the basis of damage initiation according to the ductile criterion is a phenomenological model for predicting the occurrence of damage due to void nucleation, growth and coalescence. The model assumes that the equivalent plastic deformation at the start of the damage is a function of the triaxiality of the stresses and the strain rate are indicated in the equation:

$$\bar{\varepsilon}_D^{pl}\left(\eta, \dot{\bar{\varepsilon}}^{pl}, \theta\right) \tag{13}$$

where $\eta = -\frac{p}{q}$ is the stress triaxiality, p is the pressure stress, q is the Mises equivalent stress, and $\dot{\bar{\varepsilon}}^{pl}$ is the equivalent plastic strain rate. The damage initiation criterion is met when the following condition is met:

$$w_{D=} \int \frac{d\bar{\varepsilon}^{pl}}{\bar{\varepsilon}_D^{pl}\left(\eta, \dot{\bar{\varepsilon}}^{pl}, \theta\right)} = 1 \tag{14}$$

where w_D is a state variable that increases monotonically with plastic deformation. At each increment during the analysis the incremental increase in Δw_D is computed as:

$$\Delta w_D = \frac{\Delta\bar{\varepsilon}^{pl}}{\bar{\varepsilon}_D^{pl}\left(\eta, \dot{\bar{\varepsilon}}^{pl}, \theta\right)} \tag{15}$$

The fracture energy according to the Hillerborg theory [28].was presented to model the evolution of the damage between 0 and 1, Hillerborg uses an equation (16) of the energy absorbed G_f per unit area of the crack, written as follows:

$$G_f = \int_0^{\bar{u}_f^{pl}} \sigma_y d\bar{u}^{pl} \quad \text{ou} \quad G_f = \int_{\bar{\varepsilon}_0^{pl}}^{\bar{\varepsilon}_f^{pl}} L\sigma_y d\bar{\varepsilon}^{pl} \tag{16}$$

where $\bar{u}^{pl}$ is the equivalent plastic displacement and σ_y is the elastic limit of the material, G_f is rupture energy and L is the characteristic length of the finite element, $\bar{\varepsilon}_0^{pl}$, $\bar{\varepsilon}_f^{pl}$ are the initial and final plastic deformation. The displacement damage evaluation defines damage as a function of the total or the plastic (for bulk elastic-plastic) displacement after damage initiation this type corresponds to the displacement at failure field in the equation.

$$\bar{u}_f^{pl} = \frac{2G_f^F}{\sigma_0^y} \tag{17}$$

In the stiffness degradation for the linear process, the calculation of the increment of the parameter D of the damage is based on the following equation (18).

$$D = \frac{\int_{\bar{\varepsilon}_0^{pl}}^{\bar{\varepsilon}_f^{pl}} L\sigma_y d\bar{\varepsilon}^{pl}}{G_f^F} \quad (18)$$

Before comparing the experimental and numerical aspects using the ABAQUS software, we initially created the geometry representing the tensile specimen. This 3D model creation is performed in the geometry generation module, as depicted in Fig 7. This step allows for the utilization of the graphical interface, but it's also possible to import models from CAD software such as CATIA or SolidWorks [29]. The subsequent step involves assigning material properties to various parts of the model. At this stage, pre-defined materials can be utilized, or custom materials can be generated. Following this, boundary conditions and types of loading applied to the model are defined, including temperatures. Meshing is a critical step that involves dividing the model into finite elements, with the choice of element types dependent on the model's geometry and the physics being simulated. The finite element mesh and boundary conditions are illustrated in Fig 7. A hexahedral element type comprising 5240 elements is employed in ABAQUS/Explicit. Figure.7 shows the upper part of the specimen subjected to an imposed force F of variable value along the traction axis Y while the lower part of the specimen is assumed to be embedded. Tensile tests conducted at a constant strain rate of 2 mm/min for parameter identification are simulated using the ABAQUS computational code. When the simulation is launched, ABAQUS conducts a numerical analysis to solve the mathematical equations of the model. The analysis of the simulation results, referred to as post-processing, enables the visualization of results in the form of graphs and tables. Finally, a validation step is carried out to confirm that the simulation results align with the physical reality of the problem under study and with experimental data. These steps are general and may vary depending on the complexity of the model and simulation conditions [30,31].

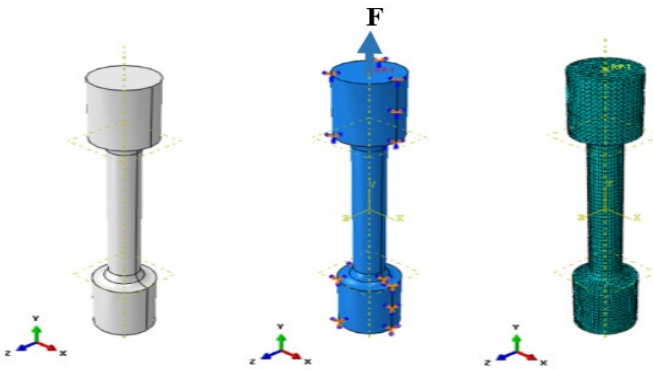

Fig. 7. Meshing of the finite element model and boundary conditions

3.6. *Comparison of Stress-strain curves for experiment and numerical results*

To verify the accuracy of the numerical model, tensile tests were conducted using ABAQUS at temperatures ranging from 350°C to 650 °C. The Stress-strain curves from both experimental tests and numerical simulations are presented in Figs 8-12. Their shapes are consistent, and the corresponding rupture points are identifiable for different temperatures. Let's take, for example, the samples subjected to 350°C and the untreated samples. The experimental results show average mechanical characteristics, with maximum stress recorded at 1650 MPa and 920 MPa,

The comparison between experimental and simulation data reveals significant agreement, with discrepancies not exceeding 15% for all studied cases. This outcome highlights the reliability and precision of the simulation results. This consistency persists for other scenarios, with discrepancies between experimental and simulation results staying below the 15% mark for stress and strain measurements. This demonstrates a high level of alignment and confirms the fidelity of the simulation model.

Overall, the combined analysis of experimental and simulation data demonstrates the accuracy of the numerical model in representing the mechanical behavior of the samples. The results align consistently with experimental observations, confirming the validity and effectiveness of this simulation method. This close correspondence bolsters confidence in the reliability of numerical simulations and their precise capability to predict the mechanical response of samples under varying conditions and temperatures.

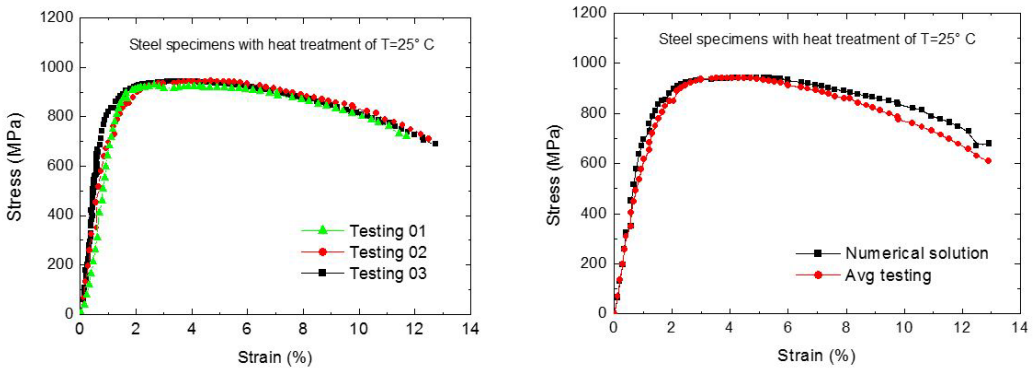

Fig. **8.** Experimental and numerical curves of the evolution of the tensile stress as a function of strain for untreated AISI 4140 steel.

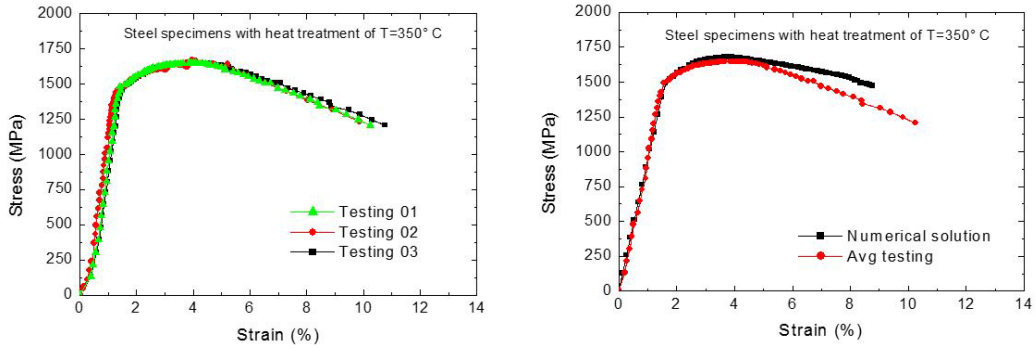

Fig. 9. Experimental and numerical curves of the evolution of the tensile stress as a function of strain for steel at tempering temperature 350 °C

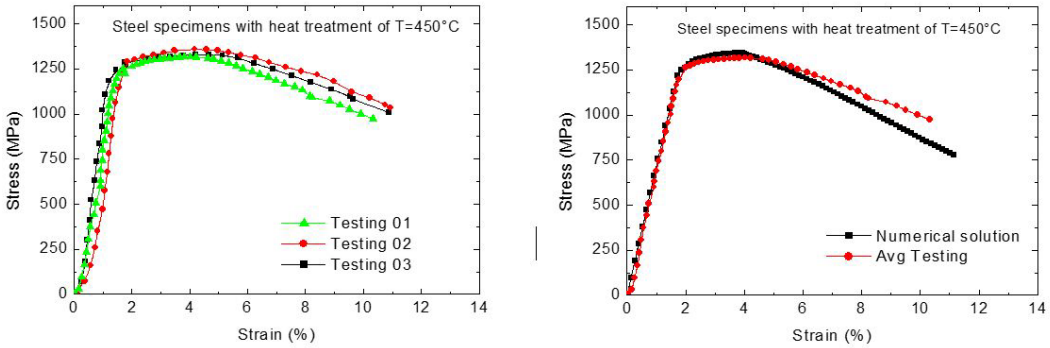

Fig. 10. Experimental and numerical curves of the evolution of the tensile stress as a function of strain for steel at tempering temperature 450 °C

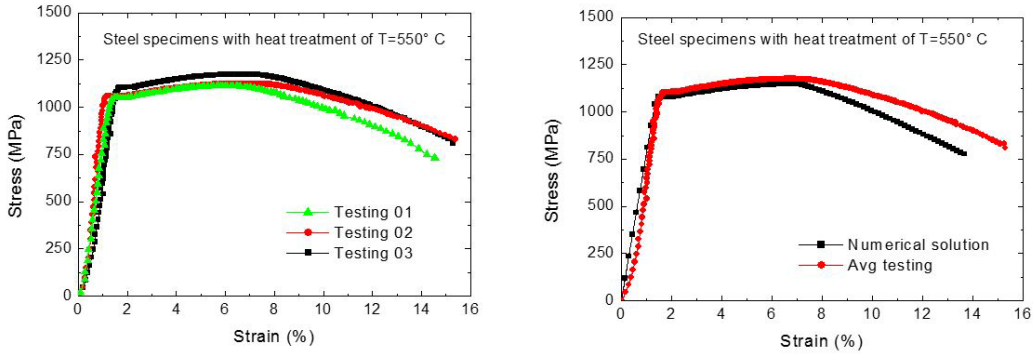

Fig. 11. Experimental and numerical curves of the evolution of the tensile stress as a function of strain for steel at tempering temperature 550 °C

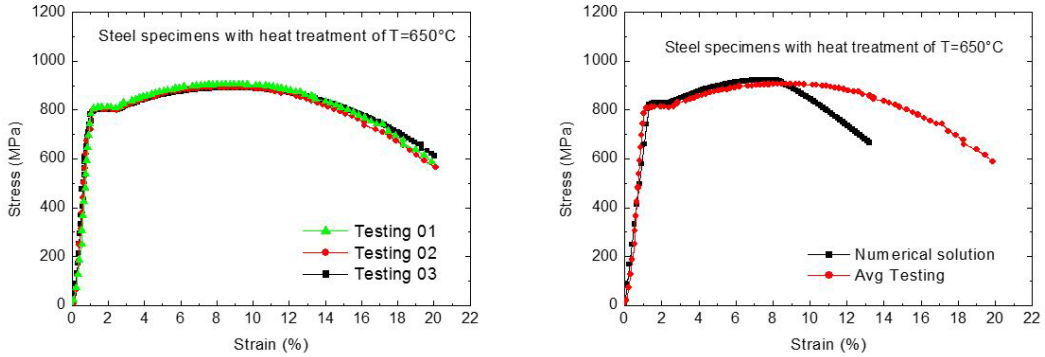

Fig. 12. Experimental and numerical curves of the evolution of the tensile stress as a function of strain for steel at tempering temperature 650 °C.

Tab 2 provides a comprehensive representation of the results obtained from distinct approaches, both experimental and numerical, exhibiting variations in stress and deformation related to temperature fluctuations during the tempering process. Within this compilation, the provided experimental values stem from an average derived from three distinct tests conducted for each sample series, each subjected to varying temperatures.

This dense table offers an in-depth comparative analysis between the experimental data and numerical outcomes, enabling the detection of notable similarities or divergences. It also highlights the discrepancies and margins of error inherent in these measurements, specifically concerning the applied thermal variations. This detailed juxtaposition of the different methodologies employed provides a holistic view of material performance at various treatment temperatures, elucidating the nuances and discrepancies between actual experimental observations and numerical predictions.

Table 2

Different results obtained experimentally, numerically and error of the Stress and strain as a function of the tempering temperature.

Temperature (°C)	Exp σ_{AVG} (MPa)	Sim σ_{MAX} (MPa)	Error E1 (%)	Exp ε_{AVG}	Sim ε_{MAX}	Error E2 (%)
Untreated steel at (25°C)	941.64	943.61	-0.20	3.89	4.06	-4.37
350	1648.2	1681.06	-1.99	3.85	3.785	1.68
450	1317.4	1344.78	-2.07	4.02	3.88	3.84
550	1174.6	1147.81	2.88	7.077	7.06	0.24
650	906.61	925.29	-2.06	8.73	8.13	6.87

4. Conclusions

This study highlights the critical importance of understanding the mechanical properties of AISI 4041 low alloy steel, particularly when subjected to specific heat treatments.

The main conclusions drawn from this work are:

• Tempering treatment is essential to alleviate the internal tensions produced after quenching and make the material hard, less fragile and ductile.

• An increase in the hardness of the material at the tempering temperature 350 ºC, it can reach a fairly high hardness of average 522HV.

• Increasing the tempering temperature, starting from 550°C, makes the material less hard and more ductile, especially at 650°C, which results in a material hardness of 304HV, lower than the as-delivered hardness of 310HV (untreated).

• The decrease in the tensile strength of the material and consequently, a reduction in the yield strength with increasing tempering temperature.

• A steel quenched followed by tempering at an elevated temperature can have a more stable microstructure and better ductility, leading to higher percent elongation.

• A high conformity between the experimental part and the numerical part in this work, where the error committed does not exceed 6.87%.

The multidisciplinary approach, combining practical experiments and numerical simulations, not only refined the precision of the results by reducing the margins of error, but also consolidated the reliability of the experimental data. These findings have a direct impact on the industry by providing essential information for designing and optimizing steel structures suitable for high temperature environments. In short, this research contributes significantly to advancing knowledge in materials and industrial mechanics, paving the way for new advances in the design of steel structures adapted to the rigors of high-temperature environments.

R E F E R E N C E S

[1]. *K. Benghalem, N. Felder, K. Loucif, P. Montmitonnet*, “Plastic deformation of 25CrMo4 steel during wear: Effect of the temperature, the normal force, the sliding velocity and the structural state”, Wear, **vol.268,** no. 3, 2010, pp. 23-40. https://doi.org/10.1016/j.wear.2009.06.036.

[2]. *M. Szala, G. Winiarski, T. Bulzak, Ł. Wójcik*, “Microstructure and Hardness of Cold Forged 42CrMo4 Steel Hollow Component with the Outer Flange”, Advances in Science and Technology Research Journal. **vol.16**, no.4.2022, pp.201–210.

[3]. *M. Duda, D. Rozumek, G. Lesiuk, M. Smolnicki, B. Babiarczuk, J. Warycha*, “Fatigue crack growth under mixed-mode I + II and I + III in heat treated 42CrMo4 steel”, Int J Fract. **vol. 234**, 2022, pp. 235–248. https://doi.org/10.1007/s10704-021-00585-0

[4]. *B. Białobrzeska, R. Jasin´ski, L. Konat, L. Szczepan´ski,* "Analysis of the properties of hardox extreme steel and possibilities of its applications in machinery", Metals. **vol.11**. no. 1, 2021, pp. 1–19. https://doi.org/10.3390/met11010162

[5].*C. Sun, P-X. Fu, H-W. Liu, H-H. Liu, N-Y. Du*, "Effect of Tempering Temperature on the Low Temperature Impact Toughness of 42CrMo4-V Steel", Metals. **vol. 4**, pp. 1-12 2018. https://doi. org/10 .3390/met8040232

[6].*M. Bayrak, F. Ozturk, M. Demirezen, Z. Evis*, "Analysis of Tempering treatment on material properties of DIN 41Cr4 and DIN 42CrMo4 Steels", Journal of Materials Engineering and Performance. **vol.16**, 2007, pp. 597-600. https://doi.org/10.1007/s11665-007-9043-1.

[7].*A. Elhadi, A. Bouchoucha, W. Jomaa, Y. Zedanc, T. Schmit, P. Bocher*, Study of Surface Wear and Damage Induced by Dry Sliding of Tempered AISI 4140 Steel against Hardened AISI 1055 Steel", Tribology in Industry, **vol. 38**, no. 4, 2016, pp. 475-485

[8].*A. Saastamoinen, A. Kaijalainen, J. Heikkala, D. Porter, P. Suikkanen*, "The effect of tempering temperature on microstructure, mechanical properties and bendability of direct-quenched low-alloy strip steel", Materials Science and Engineering: A. **vol. 730**, no.11, 2018, pp. 284-294. https://doi.org/10.1016/j.msea.2018.06.014

[9]. *M. Gogic, L. Kosec, P. Matkovic*, "The effect of tempering temperature on mechanical properties and microstructure of low alloy Cr and CrMo steel", Journal of Materials Science, **vol. 33**, 1998, pp. 395-403

[10]. *T.Fawad, N. Nausheen, A. B. Rasheed, A. Ashraf*, "Evolution of microstructure and mechanical properties during quenching and tempering of ultrahigh strength 0.3C Si-Mn-Cr-Mo low alloy steel", Journal of Materials Science, **vol. 45**, no. 6, 2010, pp. 1695-1708. DOI:10.1007/s10853-009-4160-x

[11]. *Cao.Li. Z. Guangying*, "Intergranular fracture of low-alloy cast steel". Materials Characterization,**Vol. 36**, no 2, 1996, pp. 65-72. https://doi.org/10.1016/1044-5803(95)00255-3

[12]. *O. Haiko, A. Kaijalainen, S. Pallaspuro, J. Hannula, D. Porter,T. Liimatainen and J. Kömi.* "The Effect of Tempering on the Microstructure and Mechanical Properties of a Novel 0.4C Press-Hardening Steel", Appl. Sci, **vol. 9**, no. 20, 2019, 4231, https://doi.org/10.3390/app 9204231

[13]. *S.A. Thakare, S. P. Butee, K. R. Kamble*, "Improvement in Mechanical Properties of 42CrMo4 Steel Through Novel Thermomechanical Processing Treatment", Metallography, Microstructure, and Analysis, **vol. 9**, no. 5, 2020, pp. 759– 773. https://doi. org/10.1007/s13632-020-00684-9

[14]. *T. Sharma, N. N. Kumar, R. Mondal, K. V. M. Krishna, I. Samajdar, V. Kain*, "Ductile-to-brittle transition in low-alloy steel: A combined experimental and numerical investigation". Journal of Materials Engineering and Performance. **Vol. 28**, 2019, pp. 4275-4288

[15]. *B. Buchmayr, J. S. Kirkaldy*, "Modeling of the temperature field, transformation behavior, hardness and mechanical response of low alloy steels during cooling from the austenite region" Journal of Heat Treating, **vol. 8**, 1990, pp. 127-136. DOI:10.1007/BF02831633

[16]. *J.Benzing, T. Liu Y, X. Z. Luecke, W. E. Ponge, D. Dutta, A. J. E. Wittig*, "Experimental and numerical study of mechanical properties of multi-phase medium-Mn TWIP-TRIP steel: Influences of strain rate and phase constituents", Acta materialia, **vol. 177**, 2019, pp. 250-265. https://doi.org/10.1016/j.actamat.2019.07.036

[17]. *W. Woźniak, M. Sąsiadek, T. Jachowicz, M. Edl, P. Zając*, "Studies on the Mechanical Properties of C45 Steel with Martensitic Structure after a High Tempering Process", Adv. Sci. Technol. Res. J, **vol.16**, 2022, pp. 306–315. https://doi.org/10.12913/22998624/150564

[18]. *A. Salemi, A. zadeh,* "The effect of tempering temperature on the mechanical properties and fracture morphology of a NiCrMoV steel", Materials Characterization, **vol. 59**, no. 4, 2008, pp. 484-487. https://doi.org/10.1016/j.matchar.2007.02.012

[19]. *A. Ismail, R. Zenasni. K. S. M. Amine, S. Ahmed,* "Effect of Tempering Temperature on the Mechanical Properties and Microstructure of low alloy Steel DIN 41Cr4", Jordan Journal of Mechanical and Industrial Engineering, **vol.13**, 1, 2019

[20]. *M. Sarikaya, A. K. Jhingan, G. Thomas*, "Retained austenite and tempered martensite embrittlement in medium carbon steels", Metallurgical Transactions, **vol. 14**, june1983, pp 1121–1133. doi.org/10.1007/BF02659860

[21]. *M. J. Balart, J. F. Knott*, "Low temperature fracture properties of DIN 22NiMoCr37 steel in fine-grained bainite and coarse-grained tempered embrittled martensite microstructures", Engineering Fracture Mechanics, **vol. 75**, no.8, 2008, pp.2480-2513

[22]. *Z. Ping,* "Effect of tempering temperature on microstructure and mechanical properties in new-type ultrahigh strength steel", Journal of Iron and Steel Research, International, **vol.14**, no. 5, 2007, pp 288-291. https://doi.org/10.1016/S1006-706X(08)60096-5

[23]. *T. Demir, M. Übeyli, R. Y. Orhan*, "Investigation on the ballistic impact behavior of various alloys against 7.62 mm armor piercing projectile", Materials & Design, **vol. 29**, no. 10, 2010, pp. 2009-2016. https://doi.org/10.1016/j.matdes.2008.04.010

24. *M. I. Boulifa, A. Hadji*, "Study of the influence of alloying elements on the mechanical characteristics and wear behavior of a ductile cast iron", Frattura ed Integrità Strutturale, **vol. 56**, 2021, pp. 74-83. DOI: 10.3221/IGF-ESIS.56.06.

[25]. *B. Białobrzeska*, "Effect of Alloying Additives and Microadditives on Hardenability Increase Caused by Action of Boron", Metals, **vol.11**, n 589, 2021. https://doi.org/10.3390/met11040589

[26]. Abaqus version 6.6 documentaire, partie : Abaqus Analysis user's Manual.

[27]. *L. M. Kachanov*, On the creep fracture time. Izv.Akad.Nauk USSR Otd.Tech. 1958. 8, 26-31.

[28]. *A Hillerborg, M. Modéer, P. Petersson*, "Analysis of crack formation and crack growth in concrete by means of fracture mechanics and finite elements", Cement and Concrete Research, **vol. 6**, 1976, pp. 773-782. DOI:10.1016/0008-8846(76)90007-7

[29]. *Ye X, H. Liu, L. Chen, Z. Chen, X. Pan and S. Zhang*, "Reverse innovative design - an integrated product design methodology", Computer-Aided Design, **vol. 40**, no. 7, 2008, pp. 812-827. https://doi.org/10.1016/j.cad.2007.07.006

[30]. *Shubert, M and M. Pandheeradi*, "An abaqus extension for 3-D welding simulations. in Materials Science Forum", Trans Tech Publ. Materials Science.; Forum 768-769:690-696, 2014. DOI:10.4028/www.scientific.net/MSF.768-769.690

[31]. *M. Zetterberg*, "A critical overview of machining simulations in ABAQUS", 2014.